

Six newly-discovered hot Jupiters transiting F/G stars: WASP-87b, WASP-108b, WASP-109b, WASP-110b, WASP-111b & WASP-112b^{*}

D. R. Anderson,^{1†} D. J. A. Brown,² A. Collier Cameron,³ L. Delrez,⁴ A. Fumel,⁴ M. Gillon,⁴ C. Hellier,¹ E. Jehin,⁴ M. Lendl,^{4,5} P. F. L. Maxted,¹ M. Neveu-VanMalle,^{5,6} F. Pepe,⁴ D. Pollacco,² D. Queloz,^{5,6} P. Rojo,⁷ D. Ségransan,⁵ A. M. Serenelli,⁸ B. Smalley,¹ A. M. S. Smith,^{1,9} J. Southworth,¹ A. H. M. J. Triaud,^{5,10} O. D. Turner,¹ S. Udry,⁵ and R. G. West²

¹*Astrophysics Group, Keele University, Staffordshire ST5 5BG, UK*

²*Department of Physics, University of Warwick, Coventry CV4 7AL, UK*

³*SUPA, School of Physics and Astronomy, University of St. Andrews, North Haugh, Fife KY16 9SS, UK*

⁴*Institut d'Astrophysique et de Géophysique, Université de Liège, Allée du 6 Août, 17, Bat. B5C, Liège 1, Belgium*

⁵*Observatoire de Genève, Université de Genève, 51 Chemin des Maillettes, 1290 Sauverny, Switzerland*

⁶*Cavendish Laboratory, J J Thomson Avenue, Cambridge, CB3 0HE, UK*

⁷*Departamento de Astronomía, Universidad de Chile, Santiago, Chile*

⁸*Instituto de Ciencias del Espacio (CSIC-IEEC), Facultad de Ciencias, Campus UAB, 08193, Bellaterra, Spain*

⁹*N. Copernicus Astronomical Centre, Polish Academy of Sciences, Bartycka 18, 00-716, Warsaw, Poland*

¹⁰*Department of Physics, Massachusetts Institute of Technology, Cambridge, MA 02139, USA*

Accepted Year Month Day. Received Year Month Day; in original form Year Month Day

ABSTRACT

We present the discoveries of six transiting hot Jupiters: WASP-87b, WASP-108b, WASP-109b, WASP-110b, WASP-111b and WASP-112b. The planets have masses of $0.51\text{--}2.2 M_{\text{Jup}}$ and radii of $1.19\text{--}1.44 R_{\text{Jup}}$ and are in orbits of $1.68\text{--}3.78\text{d}$ around stars with masses $0.81\text{--}1.50 M_{\odot}$.

WASP-111b is in a prograde, near-aligned ($\lambda = -5 \pm 16^\circ$), near-circular ($e < 0.10$ at 2σ) orbit around a mid-F star. As tidal alignment around such a hot star is thought to be inefficient, this suggests that either the planet migrated inwards through the protoplanetary disc or that scattering processes happened to leave it in a near-aligned orbit. WASP-111 appears to have transitioned from an active to a quiescent state between the 2012 and 2013 seasons, which makes the system a candidate for studying the effects of variable activity on a hot-Jupiter atmosphere. We find evidence that the mid-F star WASP-87 is a visual binary with a mid-G star. Two host stars are metal poor: WASP-112 has $[\text{Fe}/\text{H}] = -0.64 \pm 0.15$ and WASP-87 has $[\text{Fe}/\text{H}] = -0.41 \pm 0.10$. The low density of WASP-112 ($0.81 M_{\odot}$, $0.80 \pm 0.04 \rho_{\odot}$) cannot be matched by standard models for any reasonable value of the age of the star, suggesting it to be affected by the “radius anomaly”.

Key words: planets and satellites: individual: WASP-87b – planets and satellites: individual: WASP-108b – planets and satellites: individual: WASP-109b – planets and satellites: individual: WASP-110b – planets and satellites: individual: WASP-111b – planets and satellites: individual: WASP-112b.

1 INTRODUCTION

Advances are made in the understanding of planet formation and evolution by studying large samples of exoplanet systems and smaller subsets of well-characterised systems. There is a preponderance of giant planets around metal-rich stars and a dearth around metal-poor stars, suggestive of the core-accretion model of planet formation (Gonzalez

^{*} Based on observations made with the WASP-South photometric survey instrument at SAAO and, all located at La Silla: the 1.54-m Danish photometer under program CN2013A-159; the 60-cm TRAPPIST photometer; and the EulerCam photometer and the CORALIE spectrograph, both mounted on the 1.2-m Euler-Swiss telescope.

[†] E-mail: d.r.anderson@keele.ac.uk

1997; Santos, Israelian & Mayor 2004; Fischer & Valenti 2005). In a study of candidate transiting planets found by *Kepler* (Borucki et al. 2010), McQuillan, Mazeh & Aigrain (2013) noted a dearth of planets in orbits shorter than 2–3 d around stars with rotation periods shorter than 5–10 d, in which tidal interactions seem likely to have played a role (Lanza & Shkolnik 2014; Teitler & Königl 2014; Zhang & Penev 2014).

With coverage of bright stars ($V = 9\text{--}13$) across the whole sky (other than the galactic plane and the celestial poles) the SuperWASP photometric survey is discovering some of those inherently rare systems from which we stand, perhaps, to learn the most (Pollacco et al. 2006). For example: WASP-58 with $[\text{Fe}/\text{H}] = -0.45$ and WASP-98 with $[\text{Fe}/\text{H}] = -0.60$ are hot Jupiters orbiting metal-poor stars (Hébrard et al. 2013; Hellier et al. 2014); and WASP-18b ($10.5 M_{\text{Jup}}$), WASP-33b ($3.3 M_{\text{Jup}}$) and WASP-103b ($1.49 M_{\text{Jup}}$) are in the gap noted by McQuillan, Mazeh & Aigrain (2013): they are in ~ 1 -d orbits around rapidly rotating, bright stars ($P_{\text{rot}} < 7$ d; $V = 8.3\text{--}12.5$; Hellier et al. 2009; Collier Cameron et al. 2010; Gillon et al. 2014).

In this paper, we present the discoveries of six transiting hot Jupiters, two of which orbit metal-poor stars and three of which are in short orbits around fast rotators.

2 OBSERVATIONS

WASP-South images one third of the visible South-African sky (avoiding the galactic plane and the south pole) every ~ 10 minutes and is sensitive to the detection of giant planets transiting bright stars ($V = 9\text{--}13$). The survey and the search techniques are described in Pollacco et al. (2006) and Collier Cameron et al. (2006, 2007) and the analysis techniques are described in detail in recent WASP discovery papers (e.g. Anderson et al. 2014).

We routinely investigate the promising transit signals that we find in WASP lightcurves photometrically with the 0.6-m TRAPPIST robotic photometer and the EulerCam photometer and spectroscopically with the CORALIE spectrograph (Gillon et al. 2011; Lendl et al. 2012; Queloz et al. 2000); both EulerCam and CORALIE are mounted on the 1.2-m Euler-Swiss telescope. For three of the systems presented herein we obtained additional transit photometry with the 1.54-m Danish telescope. All the follow-up instruments are situated at La Silla.

The radial-velocity (RV) measurements computed from the CORALIE spectra exhibit variations with similar periods as the photometric dimmings seen in the WASP lightcurves and with amplitudes consistent with planetary-mass companions. The photometry and RVs are plotted for each system in Figures 1, 2, 3, 4, 5 and 6. The lack of any significant correlation between bisector span and RV supports our conclusion that the observed periodic dimmings and RV variations are caused by transiting planets (Figure 7).

With the aim of measuring the Rossiter-McLaughlin (RM) effect and thus determining the degree of alignment between the stars's rotation and the planet's orbit (e.g., Triaud et al. 2010), we took spectra with CORALIE through a transit of WASP-111b on the night beginning 2013 Aug 29 (Figure 8). Over the sequence the airmass ranged over 1.69–1.01–1.09. The star was observed simultaneously with TRAPPIST (Figure 5).

A summary of our observations is presented in Table 1 and the follow-up photometry and RVs are provided in accompanying online tables; a guide to their content and format is given in Tables 2 and 3.

We analysed the WASP lightcurves of each star to deter-

mine whether they show periodic modulation due to the combination of magnetic activity and stellar rotation (Maxted et al. 2011). We found nothing above 1 mmag for WASP-87, WASP-108 and WASP-109; the upper limit was 4 mmag for WASP-110 and 2 mmag for WASP-112. For WASP-111 we find nothing above 1 mmag for the 2006 season; the upper limit was 10 mmag for the 2007 season.

During the aperture photometry of the EulerCam images of WASP-110 the aperture encompassed a fainter star. From 46 out-of-transit images with an average stellar FWHM of $1''.3$, we measured a brightness ratio of 14.09 ± 0.15 and a separation of $4''.589 \pm 0''.006$ between WASP-110 and the nearby star. We corrected the EulerCam lightcurve for this dilution.

Table 2. TRAPPIST, EulerCam and Danish photometry of the six stars

Set	Star	Instrument	Filter	BJD(UTC) -2450000 (day)	Mag	σ_{Mag}
1	WASP-87	TRAPPIST	z'	6082.44789	0.009249	0.002876
1	WASP-87	TRAPPIST	z'	6082.44812	0.008878	0.002866
...						
...						
43	WASP-112	TRAPPIST	blue-blocking	6599.64687	0.005878	0.005179
43	WASP-112	TRAPPIST	blue-blocking	6599.64716	-0.005336	0.005165

The magnitude values are differential and normalised to the out-of-transit levels. The contamination of the WASP-110 photometry was accounted for. The uncertainties are the formal errors (i.e. they have not been rescaled). This table is available in its entirety via the CDS.

Table 1. Observations

Facility / filter	Date	N _{obs}
WASP-87:		
WASP-South / broad	2011 Jan–Jul	8943
Euler/CORALIE / spectros.	2012 May–Jul	12 RVs
TRAPPIST / z'	2012 Jun 03	631
TRAPPIST / z'	2012 Jun 08	857
TRAPPIST / z'	2012 Jul 10	609
EulerCam / Gunn r	2012 Jul 10	198
EulerCam / Gunn r	2013 Feb 17	364
Danish / R	2013 Apr 17	407
TRAPPIST / z'	2013 Apr 27	895
TRAPPIST / z'	2013 May 24	1051
WASP-108:		
WASP-South / broad	2011 Jan–2012 Jun	26769
Euler/CORALIE / spectros.	2012 Jul–2013 Aug	23 RVs
TRAPPIST / V	2013 Mar 05	729
TRAPPIST / Iz'	2013 Mar 13	977
EulerCam / Gunn r	2013 Mar 21	83
TRAPPIST / z'	2013 Apr 06	1022
Danish / R	2013 Apr 22	169
EulerCam / Gunn r	2013 Jun 04	239
TRAPPIST / z'	2014 May 15	1013
WASP-109:		
WASP-South / broad	2008 Jun–2012 Jun	23759
Euler/CORALIE / spectros.	2012 May–2013 Aug	37 RVs
EulerCam / Gunn r	2012 Jun 26	182
TRAPPIST / Iz'	2013 Mar 05	542
TRAPPIST / Iz'	2013 Apr 04	953
EulerCam / I	2013 Apr 24	253
Danish / R	2013 Apr 24	166
TRAPPIST / Iz'	2013 May 04	857
WASP-110:		
WASP-South / broad	2006 May–2012 Jun	22698
Euler/CORALIE / spectros.	2012 Jul–2013 Sep	14 RVs
EulerCam / I	2013 Aug 16	121
WASP-111:		
WASP-South / broad	2006 May–2008 Oct	9386
Euler/CORALIE / spectros.	2012 Jul–2012 Oct	28 RVs
Euler/CORALIE / spectros.	2013 Jul–2013 Sep	12 RVs
Euler/CORALIE / spectros.	2013 Aug 29	16 RVs
TRAPPIST / z'	2012 Jul 25	684
TRAPPIST / B	2012 Sep 21	562
TRAPPIST / B	2012 Oct 28	535
TRAPPIST / z'	2013 Aug 29	669
EulerCam / Gunn r	2013 Nov 04	179
WASP-112:		
WASP-South / broad	2006 May–2011 Nov	14073
Euler/CORALIE / spectros.	2012 Jul–2013 Sep	19 RVs
TRAPPIST / blue blocking [†]	2012 Nov 27	556
TRAPPIST / blue blocking [†]	2013 May 31	434
TRAPPIST / blue blocking [†]	2013 Jun 03	609
EulerCam / NGTS [‡]	2013 Aug 12	132
EulerCam / NGTS [‡]	2013 Aug 15	223
TRAPPIST / blue blocking [†]	2013 Aug 21	303
TRAPPIST / blue blocking [†]	2013 Nov 02	426

[†] www.astrodon.com/products/filters/exoplanet

[‡] Chazelas et al. (2012)

Table 3. Radial velocity measurements

Star	BJD(UTC) –2450000 (day)	RV (km s ^{–1})	σ_{RV} (km s ^{–1})	BS (km s ^{–1})
WASP-87	6068.56103	–13.8988	0.0234	0.0472
WASP-87	6069.51421	–14.4770	0.0366	–0.0319
...				
WASP-112	6537.81718	–19.4170	0.0904	–0.0498
WASP-112	6543.54834	–19.6296	0.0546	0.0312

The uncertainties are the formal errors (i.e. with no added jitter) and the WASP-111 RVs from 2012 have not been pre-whitened.

The uncertainties on bisector span (BS) is $2\sigma_{RV}$.

This table is available in its entirety via the CDS.

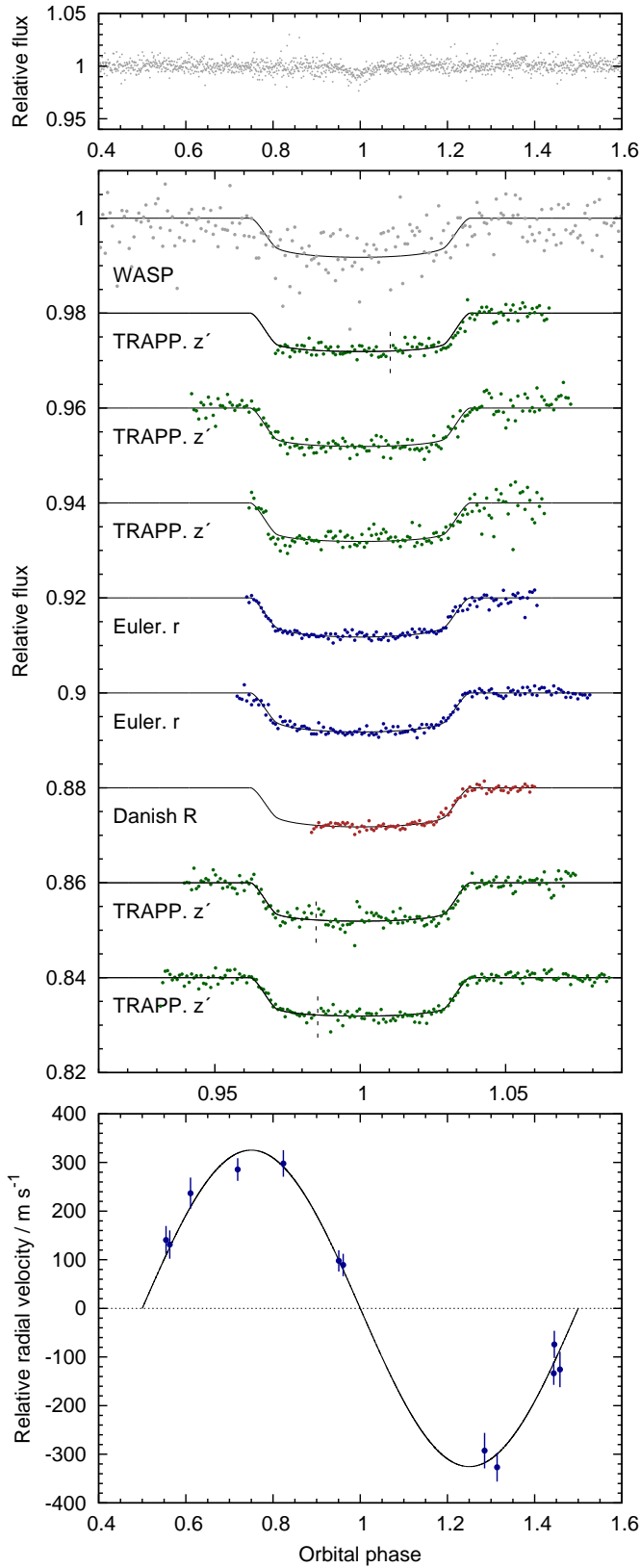


Figure 1. WASP-87b discovery data. Top panel: WASP lightcurve folded on the transit ephemeris. Second panel: Transit lightcurves from facilities and in passbands as labelled, offset for clarity. Each photometry set was binned in phase with a bin width equivalent to two minutes. The best-fitting transit model is superimposed. Vertical dashed lines indicate partitioning due to meridian flips or other issues. Third panel: The CORALIE radial velocities with the best-fitting circular Keplerian orbit model.

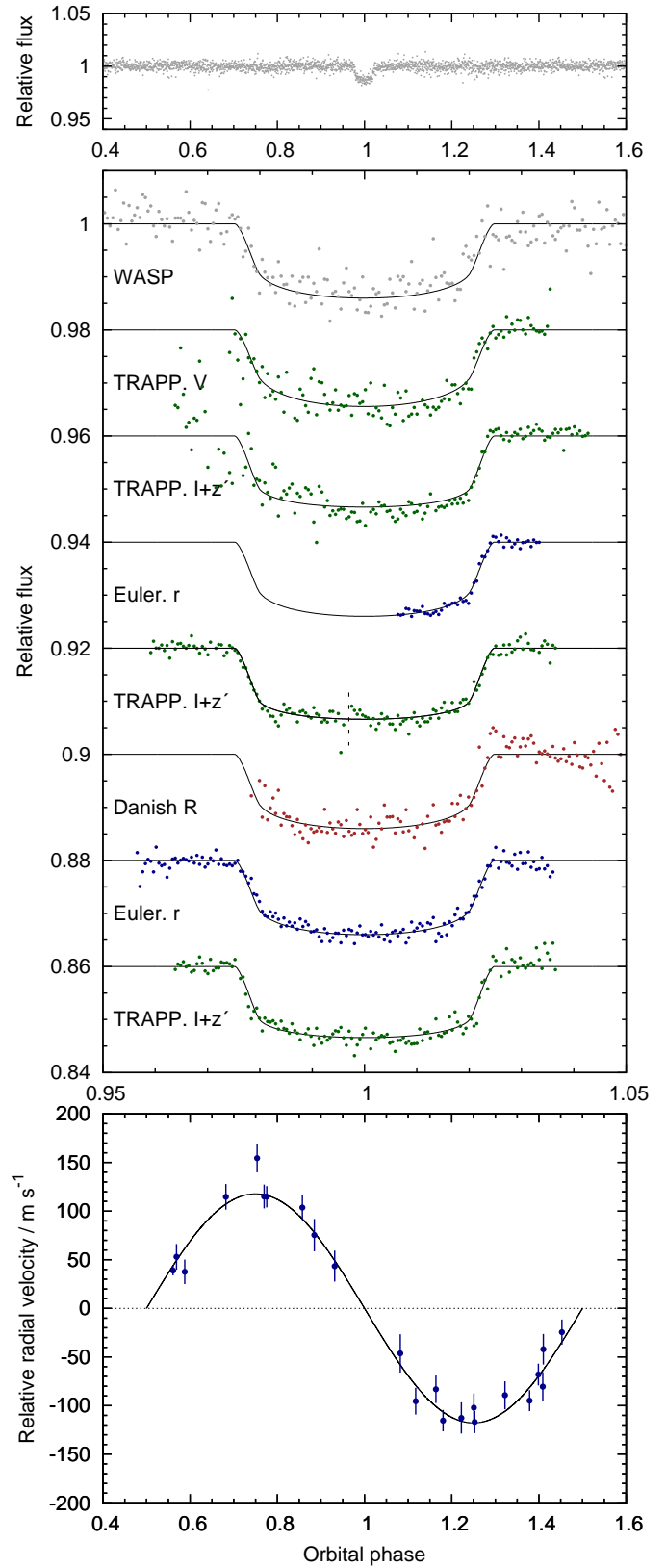


Figure 2. WASP-108b discovery data. Caption as for Fig. 1.

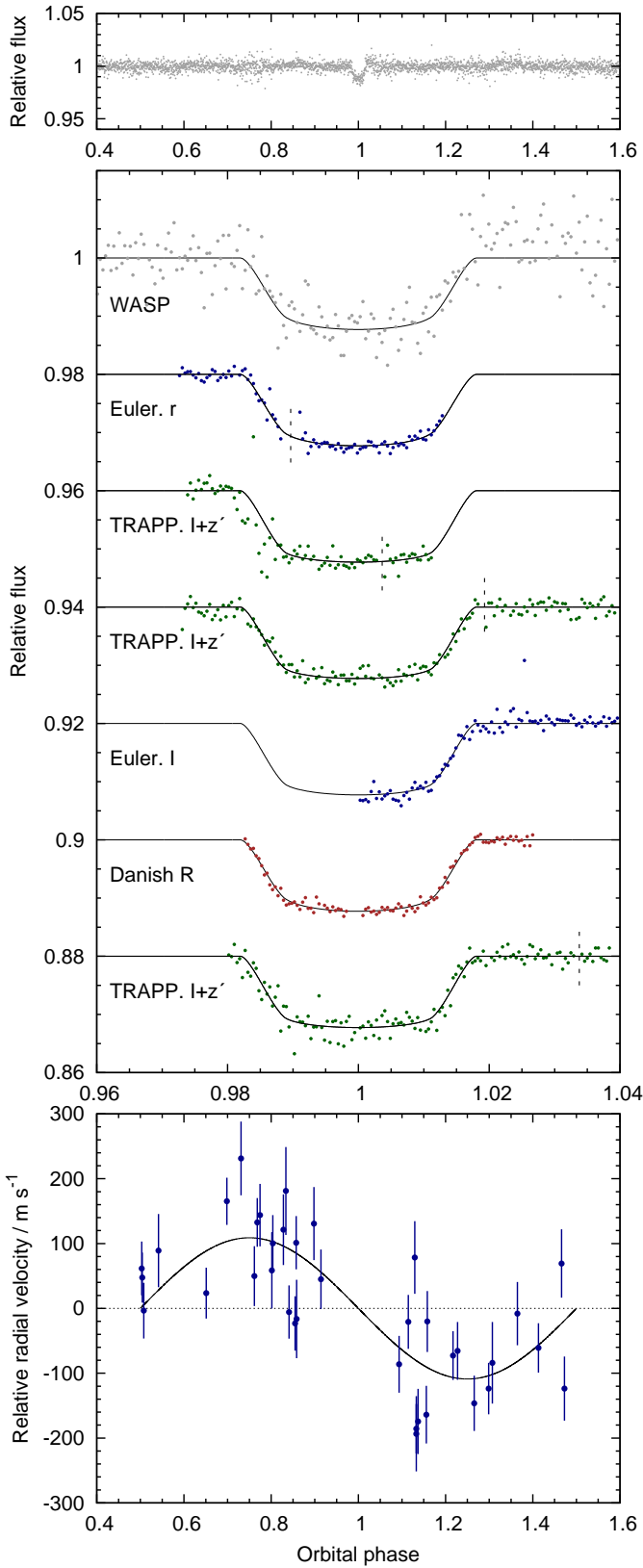


Figure 3. WASP-109b discovery data. Caption as for Fig. 1.

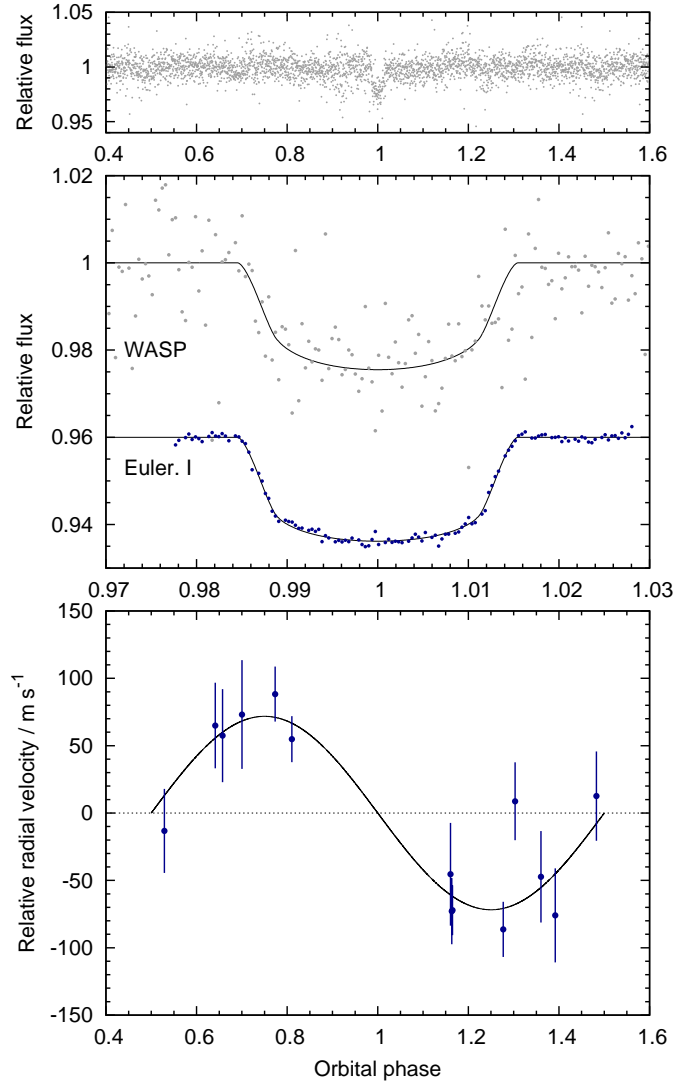


Figure 4. WASP-110b discovery data. Caption as for Fig. 1.

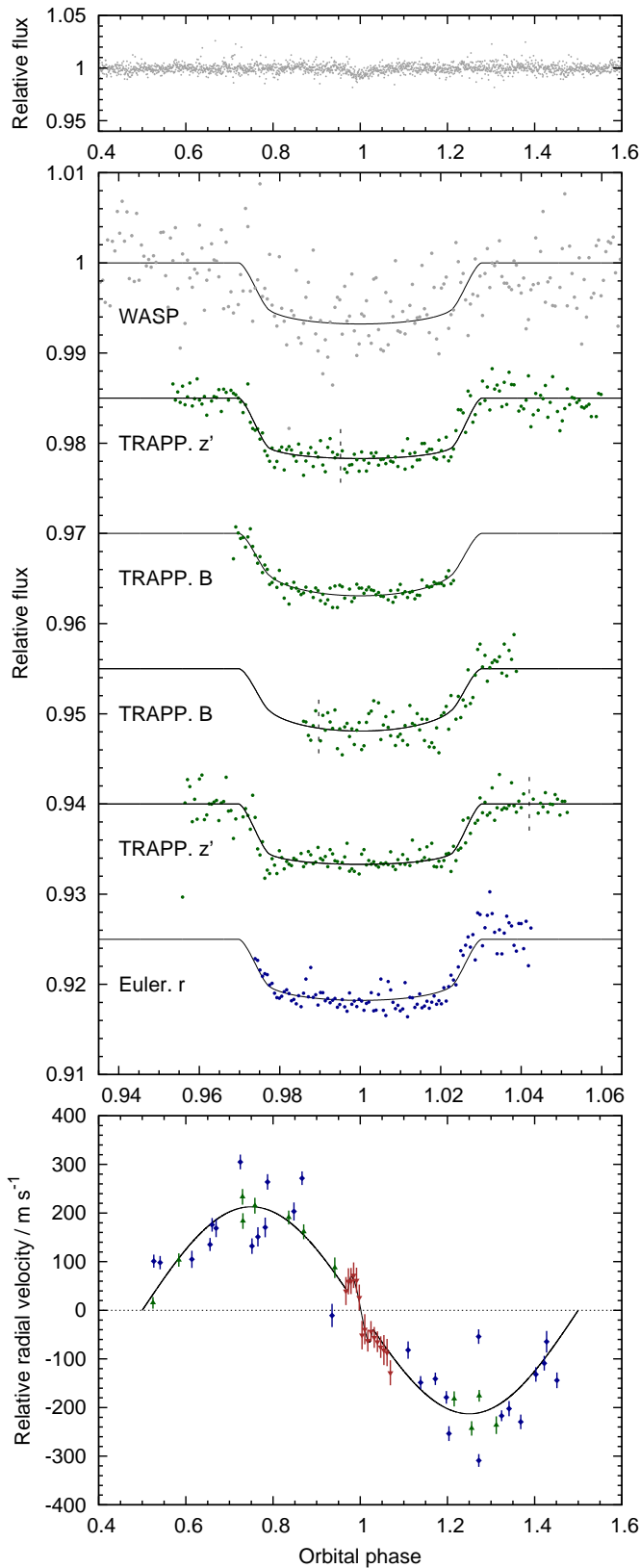


Figure 5. WASP-11b discovery data. Caption as for Fig. 1. The RVs from 2012, 2013 and the RM observation are plotted, respectively, as blue diamonds, green down-triangles and brown up-triangles.

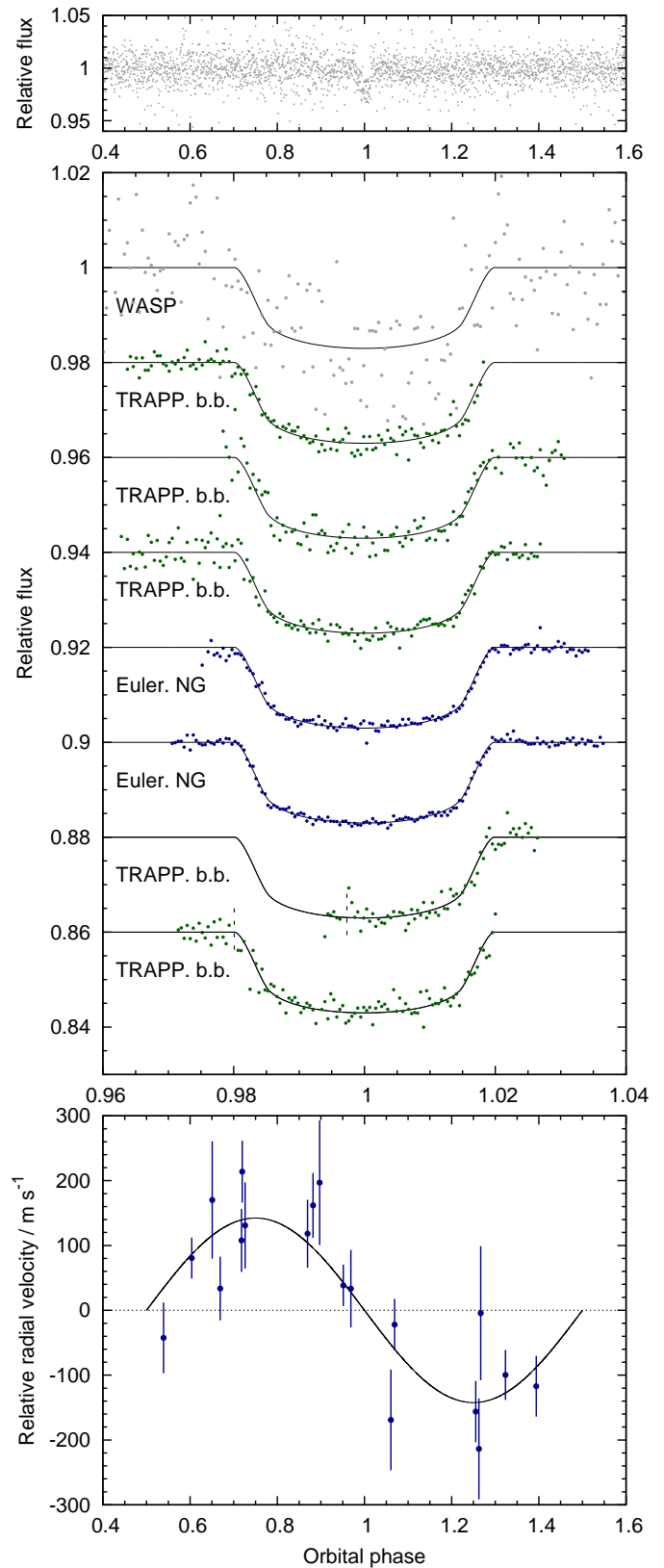


Figure 6. WASP-112b discovery data. Caption as for Fig. 1.

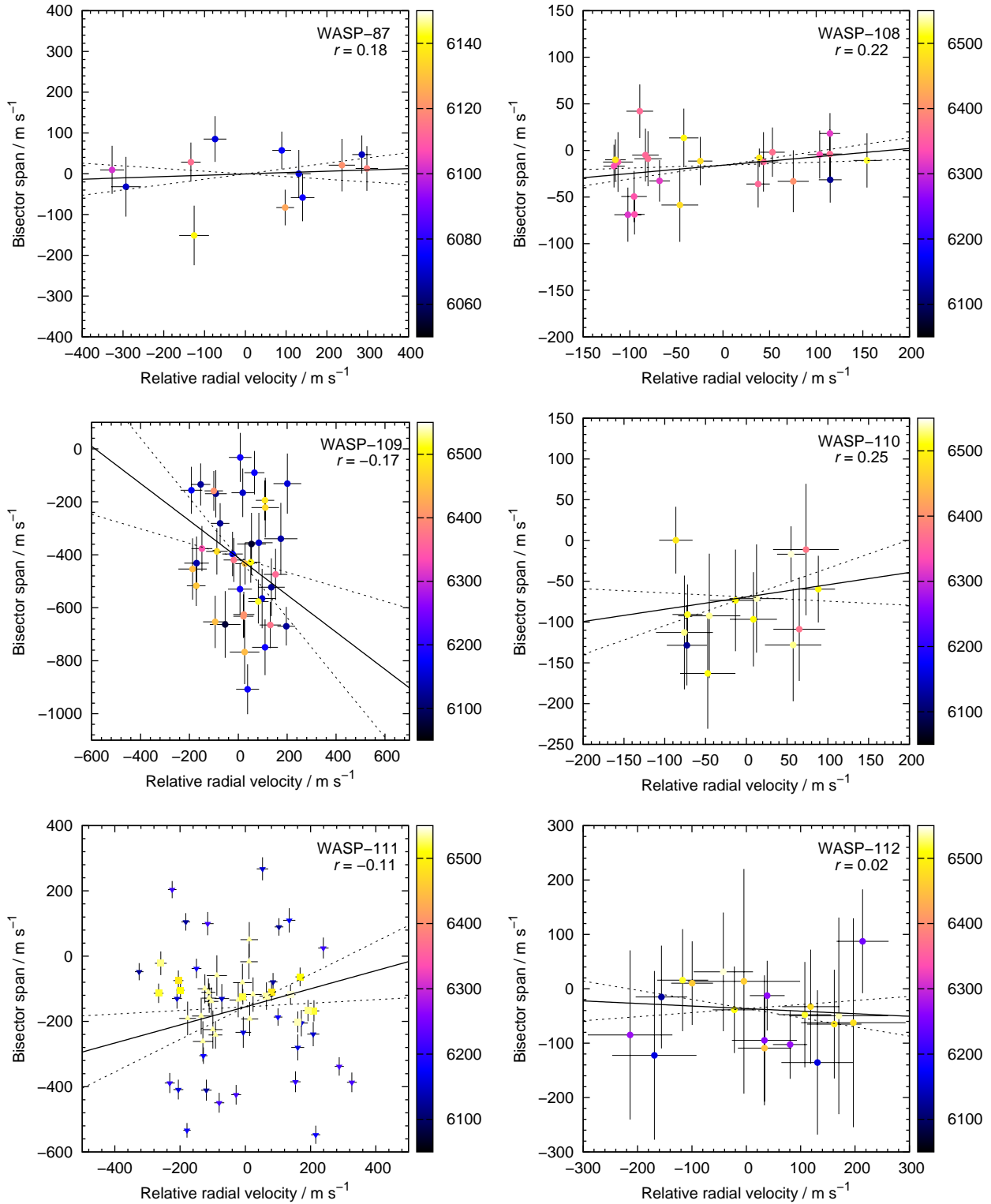


Figure 7. The lack of correlation between bisector span and radial velocity for the six stars excludes transit mimics. The solid line is the best linear fit to the data and the dotted lines are the 1- σ limits on the gradient. The Pearson product-moment correlation coefficient, r , is given in each panel. The Julian date of the observation (BJD - 2450 000) is represented by the symbol colour.

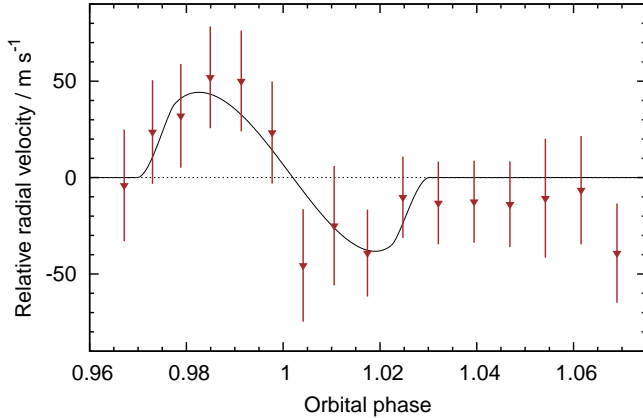


Figure 8. The Rossiter-McLaughlin effect of WASP-111b.

3 STELLAR PARAMETERS FROM SPECTRA

The individual CORALIE spectra of the host stars were co-added to produce a single spectrum per star. We performed the spectral analysis using the methods given in Doyle et al. (2013). The excitation balance of the Fe I lines was used to determine the effective temperature (T_{eff}). The surface gravity ($\log g_*$) was determined from the ionisation balance of Fe I and Fe II. The Ca I line at 6439 and the Na I D lines were also used as $\log g_*$ diagnostics. The elemental abundances were determined from equivalent width measurements of several unblended lines. The quoted error estimates include that given by the uncertainties in T_{eff} and $\log g_*$, as well as the scatter due to measurement and atomic data uncertainties. The projected stellar rotation velocity ($v \sin i_*$) was determined by fitting the profiles of several unblended Fe I lines. Values of macroturbulent velocity were assumed from the asteroseismic-based calibration of Doyle et al. (2014). The parameters obtained from the analysis are listed in Table 6.

4 SYSTEM PARAMETERS FROM COMBINED ANALYSES

We determined the parameters of each system from a simultaneous fit to the lightcurve and radial-velocity data. The fit was performed using the current version of the Markov-chain Monte Carlo (MCMC) code described by Collier Cameron et al. (2007) and Anderson et al. (2014).

The transit lightcurves were modelled using the formulation of Mandel & Agol (2002) and limb-darkening was accounted for using the four-parameter non-linear law of Claret (2000, 2004) (see Table 4 for the interpolated coefficients). The RM effect was modelled using the formulation of Hirano et al. (2011). Stellar density is determined by the transit lightcurves, but we require a constraint on stellar mass for a full characterisation of the system. For this we used the empirical mass calibration of Southworth (2011, see also the references therein).

We used the F -test approach of Lucy & Sweeney (1971) to calculate the probability that the improvement in the fit that results from fitting an eccentric orbit could have arisen by chance if the underlying orbit were circular. The values range from 0.33 (for WASP-112) to 0.93 (for WASP-87); for no system is there compelling evidence of a non-circular orbit. We thus adopt circular orbits, which Anderson et al. (2012) argue is the prudent choice for

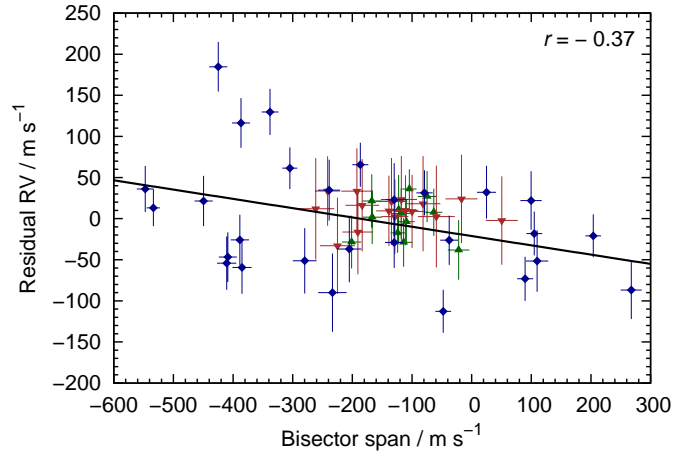


Figure 9. The correlation between residual RV and bisector span for WASP-111. The symbol shapes and colours are as in Figure 5. The fit and subsequent correction was made to the 2012 data alone; the data from 2013 are shown for reference.

short-period, \sim Jupiter-mass planets in the absence of evidence to the contrary.

The fitted parameters were T_0 , P , $(R_p/R_*)^2$, T_{14} , b , K_1 , γ , $\sqrt{v \sin i} \cos \lambda$, $\sqrt{v \sin i} \sin \lambda$, T_{eff} and $[\text{Fe}/\text{H}]$, where T_0 is the epoch of mid-transit, P is the orbital period, $(R_p/R_*)^2$ is the planet-to-star area ratio, T_{14} is the total transit duration, b is the impact parameter of the planet's path across the stellar disc, K_1 is the reflex velocity semi-amplitude, γ is the systemic velocity, $v \sin i_*$ is the sky-projected stellar rotation velocity, λ is the sky-projected obliquity, T_{eff} is the stellar effective temperature and $[\text{Fe}/\text{H}]$ is the stellar metallicity. We placed priors on both T_{eff} and $[\text{Fe}/\text{H}]$ using the spectroscopically-derived values.

To give proper weighting to each photometric data set, the uncertainties were scaled so as to obtain a photometric reduced- χ^2 of unity. To allow for flux offsets, we partitioned those TRAPPIST lightcurves involving meridian flips and the EulerCam r -band transit of WASP-109b, which was interrupted by a power cut.

To obtain a spectroscopic reduced- χ^2 of unity we added a ‘jitter’ term of 52 m s^{-1} in quadrature to the formal RV errors of WASP-109. No such addition was required in the cases of WASP-87, -108, -110 or -112. The RVs of WASP-111 were partitioned into three sets, each with its own fitted γ : the 2012 data, the 2013 data and the RM sequence. We observed greater scatter in the star's RVs from 2012, perhaps indicating a period of greater activity. We pre-whitened those data using the correlation apparent between the residual RV and bisector span (Figure 9). This resulted in a drop in RMS for the 2012 data from 68.4 m s^{-1} to 63.4 m s^{-1} . We found an offset between the corrected 2012 data and the 2013 data of $-42.56 \pm 0.90 \text{ m s}^{-1}$ and an offset of $22.0 \pm 8.8 \text{ m s}^{-1}$ between the 2013 RM sequence and the 2013 data. The jitter terms for the WASP-111 data were 55 m s^{-1} for 2012, 15 m s^{-1} for 2013 and zero for the RM sequence. During an initial MCMC we found $v \sin i_*$ from the fit to the RM effect, to range over $0\text{--}24 \text{ km s}^{-1}$ (with a best-fitting value of $9.5^{+3.4}_{-4.0} \text{ km s}^{-1}$), which is inconsistent with the spectroscopic value of $11.2 \pm 0.8 \text{ km s}^{-1}$. We thus used the spectroscopic value to place a prior on $v \sin i_*$, though we note that this barely affected the derived spin-orbit angle: we obtained $\lambda = -5 \pm 16^\circ$ with a prior and $\lambda = -5 \pm 19^\circ$ without a prior.

Table 4. Limb-darkening coefficients

Star	Instrument	Observation bands	Claret band	a_1	a_2	a_3	a_4
WASP-87	WASP / EulerCam / Danish	Broad (400–700 nm) / Gunn r / Cousins R	Cousins R	0.358	0.740	−0.600	0.165
WASP-87	TRAPPIST	Sloan z'	Sloan z'	0.447	0.282	−0.190	0.012
WASP-108	WASP / EulerCam / Danish	Broad (400–700 nm) / Gunn r / Cousins R	Cousins R	0.593	−0.049	0.464	−0.274
WASP-108	TRAPPIST	Cousins I + Sloan z' / Sloan z'	Sloan z'	0.685	−0.401	0.668	−0.331
WASP-108	TRAPPIST	Johnson V	Johnson V	0.514	0.145	0.383	−0.248
WASP-109	WASP / EulerCam / Danish	Broad (400–700 nm) / Gunn r / Cousins R	Cousins R	0.499	0.396	−0.226	0.025
WASP-109	TRAPPIST	Cousins I + Sloan z'	Sloan z'	0.589	−0.027	0.120	−0.010
WASP-109	EulerCam	Cousins I	Cousins I	0.569	0.093	0.025	−0.066
WASP-110	WASP	Broad (400–700 nm)	Cousins R	0.657	−0.456	1.100	−0.529
WASP-110	EulerCam	Cousins I	Cousins I	0.737	−0.666	1.156	−0.529
WASP-111	WASP / EulerCam	Broad (400–700 nm) / Gunn r	Cousins R	0.488	0.454	−0.310	0.064
WASP-111	TRAPPIST	Sloan z'	Sloan z'	0.582	0.017	0.055	−0.071
WASP-111	TRAPPIST	Johnson B	Johnson B	0.344	0.676	−0.178	−0.003
WASP-112	WASP / EulerCam / TRAPPIST	Broad (400–700 nm) / NGTS / blue block.	Cousins R	0.449	0.256	0.196	−0.188

5 COMPARISON TO EVOLUTIONARY MODELS

We used a Markov chain Monte Carlo method to calculate the posterior distribution for the mass and age of each host star based on a comparison of the observed values of ρ_* , T_{eff} and $[\text{Fe}/\text{H}]$ to a grid of stellar models. The method is described in detail in Maxted, Serenelli & Southworth (2014). The stellar models were calculated using the GARSTEC stellar evolution code (Weiss & Schlattl 2008) and the methods used to calculate the stellar model grid are described in Serenelli et al. (2013).

To estimate the likelihood of observing the data $\mathbf{d} = (T_{\text{eff}}, [\text{Fe}/\text{H}], \rho_*)$ for a given model $\mathbf{m} = (M_*, \tau_*, [\text{Fe}/\text{H}])$ (where τ_* is the age of the star) we use $\mathcal{L}(\mathbf{d}|\mathbf{m}) = \exp(-\chi^2/2)$, where

$$\chi^2 = \frac{(T_{\text{eff}} - T_{\text{eff,obs}})^2}{\sigma_T^2} + \frac{([\text{Fe}/\text{H}]_s - [\text{Fe}/\text{H}]_{s,\text{obs}})^2}{\sigma_{[\text{Fe}/\text{H}]}^2} + \frac{(\rho_* - \rho_{*,\text{obs}})^2}{\sigma_\rho^2}.$$

In this expression for χ^2 observed quantities are denoted by the subscript ‘obs’, their standard errors are σ_T , etc., and other quantities are derived from the model grid using spline interpolation. We use the Metropolis-Hastings algorithm to produce a Markov chain of 50,000 steps with the Bayesian probability distribution $p(\mathbf{m}|\mathbf{d})$ (Tegmark et al. 2004). We assume uniform priors for the mass, age and composition of the star over the range of valid grid values ($M_* = 0.6 M_\odot$ to $2.0 M_\odot$, $[\text{Fe}/\text{H}] = -0.75$ to 0.55 and $\tau_* = 0.1$ Gyr to either 17.5 Gyr or the age at which the stellar radius first exceeds $3R_\odot$). The results of this Bayesian analysis are given in Table 5; there is good agreement with the stellar masses derived in the MCMC analyses (compare with Table 6).

For WASP-112, using our standard grid of stellar models we found that the probability that the age of this star is less than the age of the Galactic disc (10 Gyr, Cojocaru et al. 2014) is $p(\tau_* < 10 \text{ Gyr}) = 0.04$. This makes it likely that this star is affected by the ‘radius anomaly’: some late-type stars appear to be significantly larger than predicted by standard stellar models (Hoxie 1973; Popper 1997; López-Morales 2007; Spada et al. 2013). It has been proposed that this is due to the magnetic field reducing the efficiency of energy transport by convection, a phenomenon that can be approximated by reducing the mixing length parameter used in the model (Feiden & Chaboyer 2013; Chabrier, Gallardo & Baraffe 2007). The mixing length parameter used to calculate our model grid is $\alpha_{\text{MLT}} = 1.78$. With this value of α_{MLT} GARSTEC reproduces the observed properties of the present

Table 5. Bayesian mass and age estimates for the host stars Columns 2 and 3 give the maximum-likelihood estimates of the age and mass, respectively. The chi-squared value for the the best fit is given in column 4. Columns 5 and 6 give the mean and standard deviation of the posterior age and mass distribution, respectively.

Star	τ_b [Gyr]	M_b [M_\odot]	χ^2	$\langle \tau_* \rangle$ [Gyr]	$\langle M_* \rangle$ [M_\odot]
WASP-87	3.4	1.20	0.05	3.8 ± 0.8	1.20 ± 0.08
WASP-108	4.3	1.11	0.21	4.6 ± 1.9	1.10 ± 0.07
WASP-109	2.4	1.20	0.27	2.6 ± 0.9	1.19 ± 0.06
WASP-110	8.4	0.87	0.29	8.6 ± 3.5	0.87 ± 0.05
WASP-111	2.6	1.40	0.18	2.6 ± 0.6	1.41 ± 0.07
WASP-112 ^a	12.5	0.80	0.08	10.6 ± 3.0	0.83 ± 0.05

^a Assuming $\alpha_{\text{MLT}} = 1.22$

day Sun. There is currently no practical way to select the correct value of α_{MLT} for a magnetically active star other than to find the range of this parameter that gives plausible results. Accordingly, we calculated a Markov chain for the observed parameters of WASP-112 using stellar models with $\alpha_{\text{MLT}} = 1.22$, for which value we find $p(\tau_* < 10 \text{ Gyr}) = 0.43$. The fit to the observed density and effective temperature of WASP-112 is shown in Fig. 10.

6 THE PLANETARY SYSTEMS

6.1 The WASP-87 system

WASP-87b is a $2.2 M_{\text{Jup}}$, $1.39 R_{\text{Jup}}$ planet in a 1.68-day orbit around a $V = 10.6$, metal-poor F5 star. With $[\text{Fe}/\text{H}] = -0.41$, WASP-87 is one of the most metal-poor stars found to host a giant planet. From $v \sin i_*$ and R_* we calculated a stellar rotation period of $P_{\text{rot}} < 8.6 \pm 0.7 \text{ d}$. Together with the orbital period, P_{orb} , of 1.68 d, this places WASP-87 in the sparsely-populated region of $P_{\text{rot}}-P_{\text{orb}}$ space identified by McQuillan, Mazeh & Aigrain (2013). The radius we derived for WASP-87b is smaller by $0.27 R_{\text{Jup}}$ than predicted by the empirical relation of Enoch, Collier Cameron & Horne (2012) based on the planet’s T_{eq} , M_p and $[\text{Fe}/\text{H}]$. The average difference between the predicted and observed radii for the calibration sample of Enoch, Collier Cameron & Horne (2012) was $0.11 R_{\text{Jup}}$.

There is another star, 2MASS 12211848–5250332, located

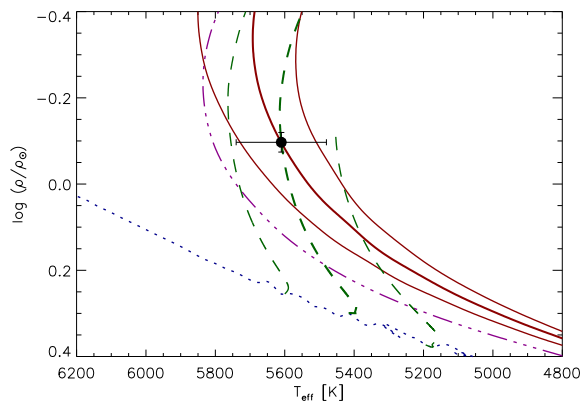


Figure 10. Mean stellar density versus effective temperature for WASP-112 compared to stellar evolution models assuming $\alpha_{\text{MLT}} = 1.22$ and the best-fitting value of $[\text{Fe}/\text{H}]$. Isochrones (solid lines, red) are shown for the best-fitting age and also for age $\pm 1\sigma$. Similarly, evolution tracks (dashed lines, green) are shown for the best-fitting mass and $\pm 1\sigma$. The zero-age main sequence is also shown (dotted line, cyan). For comparison, an isochrone is shown assuming the standard value of $\alpha_{\text{MLT}} = 1.78$ and an age of 14.8 Gyr (dot-dash line, magenta).

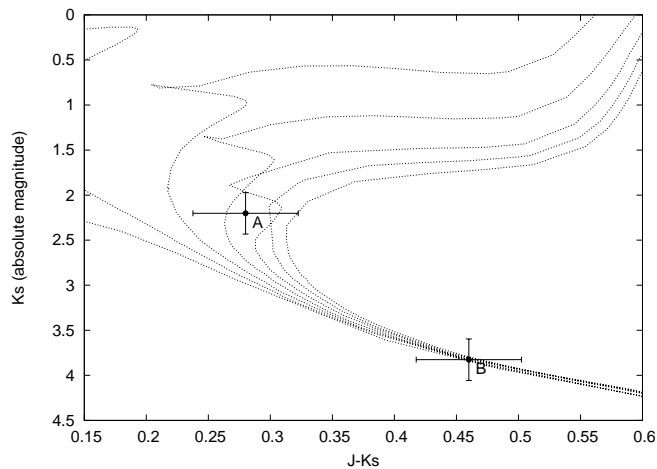


Figure 11. Colour-magnitude diagram for WASP-87A+B. The isochrones range from 0 to 6 Gyr in 1-Gyr increments (Marigo et al. 2008).

8'2 to the south-east of WASP-87A with $V_{\text{mag}} = 12.8$ and $K_{\text{mag}} = 11.2$. From its spectral energy distribution we found $T_{\text{eff}} = 5700 \pm 150$ K. The nearby star's proper motion in UCAC4 ($\mu_{\text{RA}} = 1.3 \pm 1.7$ mas/yr, $\mu_{\text{Dec}} = -2.9 \pm 2.0$ mas/yr) and that of WASP-87A ($\mu_{\text{RA}} = -3.4 \pm 0.8$ mas/yr, $\mu_{\text{Dec}} = 13.9 \pm 2.1$ mas/yr) are similar. From three CORALIE spectra of the nearby star we measured its radial velocity to be -13.348 ± 0.013 km s $^{-1}$, which is close to the systemic velocity of WASP-87A (-14.1845 ± 0.0079 km s $^{-1}$). We interpret this as suggesting that WASP-87A and the nearby star, which we tentatively name WASP-87B, comprise a bound system. We constructed a colour-magnitude diagram using 2MASS magnitudes that indicates a system age of 3–4 Gyr (Figure 11). This is in good agreement with the age of 3.8 ± 0.6 Gyr that we derived from an evolutionary analysis.

6.2 The WASP-108 system

WASP-108b is a $0.89-M_{\text{Jup}}$, $1.28-R_{\text{Jup}}$ planet in a 2.68-day orbit around a $V = 11.2$, $[\text{Fe}/\text{H}] = +0.05$, F9 star. From an evolutionary analysis we find the stellar age to be 4.6 ± 1.9 Gyr.

6.3 The WASP-109 system

WASP-109b is a $0.9-M_{\text{Jup}}$, $1.44-R_{\text{Jup}}$ planet in a 3.32-day orbit around a $V = 11.4$, $[\text{Fe}/\text{H}] = -0.22$, F4 star. Our evolutionary analysis suggests an age of 2.6 ± 0.9 Gyr. From $v \sin i_*$ and R_* we calculated a stellar rotation period of $P_{\text{rot}} < 4.4 \pm 0.3$ d. Together with the orbital period, P_{orb} , of 3.32 d, this places WASP-109 in the sparsely-populated region of $P_{\text{rot}}-P_{\text{orb}}$ space identified by McQuillan, Mazeh & Aigrain (2013).

6.4 The WASP-110 system

WASP-110b is a $0.51-M_{\text{Jup}}$, $1.24-R_{\text{Jup}}$ planet in a 3.78-day orbit around a $V = 12.3$, $[\text{Fe}/\text{H}] = -0.06$, G9 star. Our evolutionary analysis suggests a stellar age of 8.6 ± 3.5 Gyr. Our radius for WASP-110b ($1.38 R_{\text{Jup}}$) is smaller by $0.22 R_{\text{Jup}}$ than predicted by the empirical relation of Enoch, Collier Cameron & Horne (2012). There is a star 14 times fainter than WASP-110 separated by $4'6$. Further observations are required to ascertain whether they comprise a visual binary or are merely a line-of-sight coincidence.

6.5 The WASP-111 system

WASP-111b is a $1.83-M_{\text{Jup}}$, $1.44-R_{\text{Jup}}$ planet in a 2.31-day orbit around a $V = 10.3$, $[\text{Fe}/\text{H}] = +0.08$, F5 star. Our evolutionary analysis suggests an age of 2.6 ± 0.6 Gyr. With $P_{\text{rot}} < 8.4 \pm 0.7$ d and $P_{\text{orb}} = 2.31$ d, WASP-111 also occupies the sparsely-populated region of $P_{\text{rot}}-P_{\text{orb}}$ space identified by McQuillan, Mazeh & Aigrain (2013). Similar to WASP-87b and WASP-110b, we derived a radius for WASP-111b that is $0.23 R_{\text{Jup}}$ smaller than predicted by the empirical relation of Enoch, Collier Cameron & Horne (2012). The masses and irradiation levels of both WASP-87b and WASP-111b are similar, but their metallicities differ.

From a fit to the RM effect (Figure 8), we find WASP-111b to be in a prograde orbit, with a sky-projected stellar obliquity λ of $-5 \pm 16^\circ$. If the stellar spin axis is near-aligned with the sky plane then WASP-111b is in a near-aligned orbit, i.e. the true obliquity $\Psi \sim \lambda$. As $T_{\text{eff}} = 6400 \pm 150$ K, WASP-111 is expected to have little convective envelope and so to weakly tidally interact with WASP-111b (Winn et al. 2010). This would suggest either that the planet migrated via alignment-preserving tidal interaction with a proto-planetary disc or via scattering processes that, by chance, left the planet in a near-aligned orbit (e.g. Anderson et al. 2014).

It appears that WASP-111 was active when we observed it with CORALIE in July to October of 2012, then quiescent during July to September of the following year. The scatter in the bisector span and the FWHM of the CCF, and in the RV residuals was much larger in 2012 than in 2013 (Figure 12). This indicates that WASP-111 ($T_{\text{eff}} \sim 6400$ K) undergoes activity cycles like the Sun, and may have a shorter cycle period like τ Boo ($T_{\text{eff}} \sim 6300$ K; Nordström et al. 2004). In 2012, the peak to peak variation in residual RV, CCF bisector span and CCF FWHM was, respectively, 297 m s $^{-1}$, 815 m s $^{-1}$ and 1039 m s $^{-1}$. The corresponding values during the RM sequence of 2013 Aug 29 were factors of a few smaller: 60 m s $^{-1}$, 312 m s $^{-1}$ and 364 m s $^{-1}$. Perhaps this information, together with the size of the planet, could be used

to determine the effective size and intensity of the active regions (e.g. Dumusque, Boisse & Santos 2014). The variable nature of the stellar activity of WASP-111, the star's brightness and the planet's close orbit make it an ideal candidate for studying the effects of variable activity on a hot-Jupiter atmosphere.

6.6 The WASP-112 system

WASP-112b is a $0.9-M_{\text{Jup}}$, $1.19-R_{\text{Jup}}$ planet in a 3.04-day orbit around a $V = 13.3$, metal-poor star ($[\text{Fe}/\text{H}] = -0.64$). The T_{eff} of 5610 K implies a spectral type of G6, though our derived stellar mass of $0.81 M_{\odot}$ is suggestive of K0V. As a check of our spectroscopic T_{eff} , we used the infrared flux method (IRFM) of Blackwell & Shallis (1977) and obtained $T_{\text{eff}} = 5760 \pm 130$ K, which is even more discrepant with our derived stellar mass.

The low density of WASP-112 cannot be matched by standard stellar models for any reasonable value of age (Section 5). This could be due to unreliable spectral parameters as, due to the faintness of the star, the S/N of the coadded CORALIE spectrum is only $\sim 50:1$. We found that the MCMC method of Macted, Serenelli & Southworth (2014) gave a good fit for $[\text{Fe}/\text{H}] = 0.2 \pm 0.2$ (cf. the spectroscopic value of -0.64 ± 0.15) when using the IRFM T_{eff} , ρ_{\star} from Table 6, and with an upper limit on the age of 10 ± 1 Gyr. Alternatively, we can match the properties of this star if we assume a much lower value for the mixing length parameter in the models than the value $\alpha_{\text{MLT}} = 1.78$ that comes from calibrating the models using the present-day properties of the Sun. There is some evidence that low values of α_{MLT} are appropriate for models of K-dwarfs like WASP-112 if they are magnetically active. Magnetic activity is a consequence of rapid rotation in low mass stars and can be detected through chromospheric emission lines, e.g., Ca II H- and K-line emission, or modulation of the light curve due to star spots. However, WASP-112 does not show any strong signal of star spot activity in its light curve, and the projected rotation velocity of this star is very low. We can exclude strong Ca II H+K emission, but the CORALIE spectra are too low S/N to be sensitive to weak emission. It may be that WASP-112 is a rapidly rotating star, but that the rotation axis is oriented towards the Earth so that the projected rotational velocity is low and the modulation in brightness due to the changing visibility of star spots with rotation is negligible. If this is the case, then the orbit of WASP-112b must be misaligned with the rotation axis of the star, i.e. WASP-112b is on a polar orbit around WASP-112. This hypothesis can be directly tested using observations of the RM effect.

WASP-112 has the lowest metallicity of any star known to be orbited by a Jupiter-like planet; with $[\text{Fe}/\text{H}] = -0.60$, WASP-98 is the next most metal-poor giant-planet host. If stellar metallicity is representative of protoplanetary-disc metallicity, the discs of these two stars would have contained relatively little solid material. Further, both stars are low mass (WASP-98 has $0.69 \pm 0.06 M_{\odot}$ and WASP-112 has $0.81 \pm 0.07 M_{\odot}$) so their protoplanetary discs are expected to have been relatively low mass. Both the low metallicity and the low mass of these two stars may pose problems for the model of formation of giant planets via core accretion.

ACKNOWLEDGEMENTS

WASP-South is hosted by the South African Astronomical Observatory; we are grateful for their ongoing support and assistance. Funding for WASP comes from consortium universities and from

the UK's Science and Technology Facilities Council. The Euler-Swiss telescope is supported by the Swiss National Science Foundation. TRAPPIST is funded by the Belgian Fund for Scientific Research (Fond National de la Recherche Scientifique, FNRS) under the grant FRFC 2.5.594.09.F, with the participation of the Swiss National Science Foundation (SNF). L. Delrez is a FNRS/FRIA Doctoral Fellow. M. Gillon and E. Jehin are FNRS Research Associates. P. Rojo is supported by Fondecyt grant #1120299. A. Serenelli acknowledges support by the MICINN grants AYA2011-24704 and ESP2013-41268-R. A. H. M. J. Triaud is a Swiss National Science Foundation fellow under grant number P300P2-147773.

REFERENCES

- Anderson D. R. et al., 2014, MNRAS, 445, 1114
 —, 2012, MNRAS, 422, 1988
 —, 2014, A&A, submitted, arXiv:1402.1482
 Asplund M., Grevesse N., Sauval A. J., Scott P., 2009, ARA&A, 47, 481
 Blackwell D. E., Shallis M. J., 1977, MNRAS, 180, 177
 Borucki W. J. et al., 2010, Science, 327, 977
 Chabrier G., Gallardo J., Baraffe I., 2007, A&A, 472, L17
 Chazelas B. et al., 2012, in Society of Photo-Optical Instrumentation Engineers (SPIE) Conference Series, Vol. 8444, Society of Photo-Optical Instrumentation Engineers (SPIE) Conference Series
 Claret A., 2000, A&A, 363, 1081
 —, 2004, A&A, 428, 1001
 Cojocaru R., Torres S., Isern J., García-Berro E., 2014, A&A, 566, A81
 Collier Cameron A. et al., 2010, MNRAS, 407, 507
 —, 2006, MNRAS, 373, 799
 —, 2007, MNRAS, 380, 1230
 Doyle A. P., Davies G. R., Smalley B., Chaplin W. J., Elsworth Y., 2014, MNRAS, 444, 3592
 Doyle A. P. et al., 2013, MNRAS, 428, 3164
 Dumusque X., Boisse I., Santos N. C., 2014, A&A, accepted, arXiv:1409.3594
 Enoch B., Collier Cameron A., Horne K., 2012, A&A, 540, A99
 Feiden G. A., Chaboyer B., 2013, ApJ, 779, 183
 Fischer D. A., Valenti J., 2005, ApJ, 622, 1102
 Gillon M. et al., 2014, A&A, 562, L3
 —, 2011, A&A, 533, A88
 Gonzalez G., 1997, MNRAS, 285, 403
 Gray D. F., 2008, The Observation and Analysis of Stellar Photospheres. Cambridge University Press
 Hébrard G. et al., 2013, A&A, 549, A134
 Hellier C. et al., 2014, MNRAS, 440, 1982
 —, 2009, Nature, 460, 1098
 Hirano T., Suto Y., Winn J. N., Taruya A., Narita N., Albrecht S., Sato B., 2011, ApJ, 742, 69
 Hoxie D. T., 1973, A&A, 26, 437
 Lanza A. F., Shkolnik E. L., 2014, MNRAS, 443, 1451
 Lendl M. et al., 2012, A&A, 544, A72
 López-Morales M., 2007, ApJ, 660, 732
 Lucy L. B., Sweeney M. A., 1971, AJ, 76, 544
 Mandel K., Agol E., 2002, ApJ, 580, L171
 Marigo P., Girardi L., Bressan A., Groenewegen M. A. T., Silva L., Granato G. L., 2008, A&A, 482, 883
 Macted P. F. L. et al., 2011, PASP, 123, 547

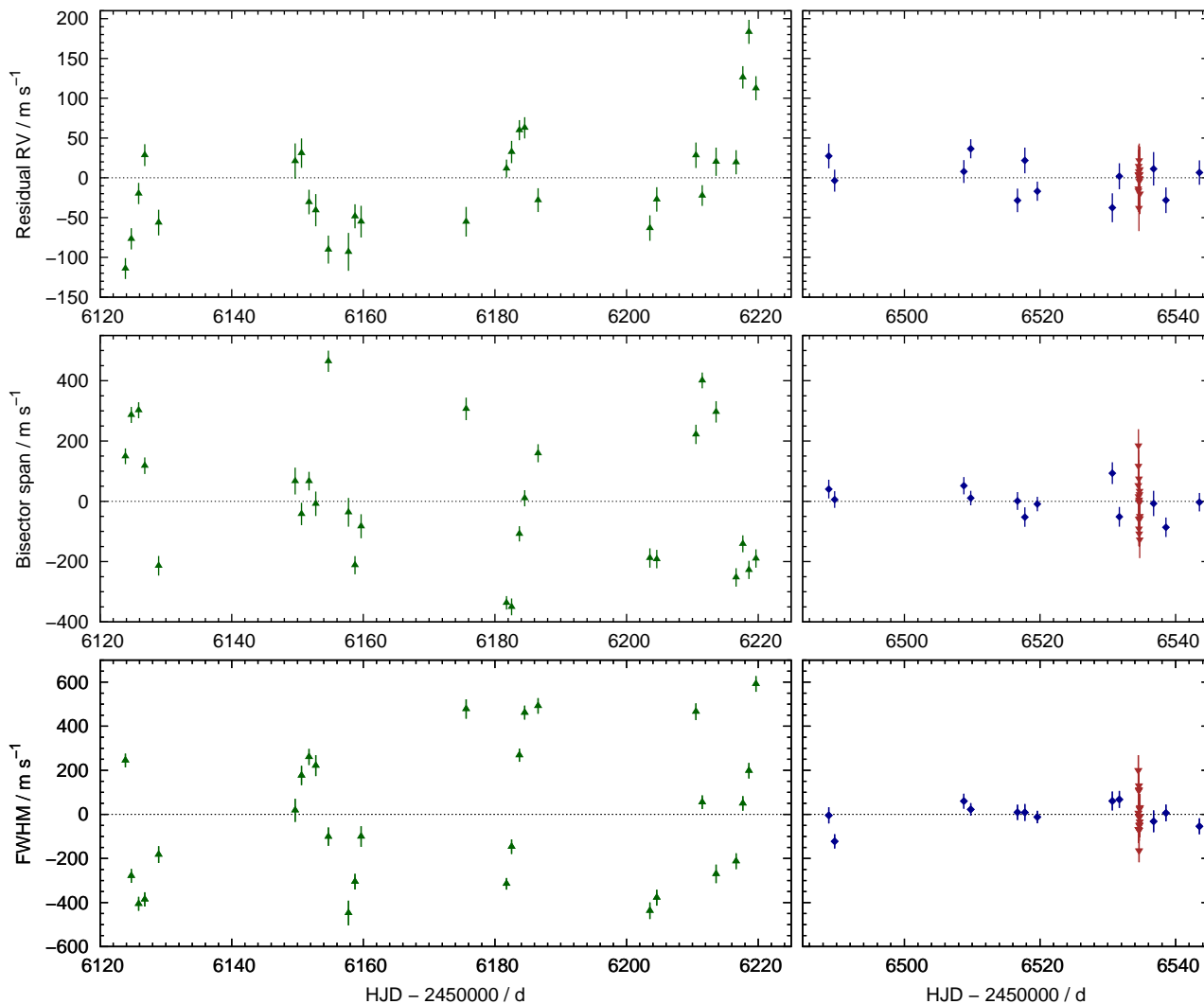


Figure 12. The variable activity of WASP-111. The panels to the left show the data from 2012 Jul 14–Oct 19 and the panels to the right show the data from 2013 Jul 14–Sep 8, including the transit observation of Aug 29. The symbol shapes and colours are as in Figure 5. The weighted mean was subtracted from each dataset for the bisector span and FWHM plots. *Top panels:* Residuals about a fit to the RVs of a circular Keplerian orbit. The RVs were partitioned into three sets: 2012 (not pre-whitened), 2013 and the RM effect. *Middle panels:* Bisector span of the CCF. *Bottom panels:* FWHM of the CCF.

- Maxted P. F. L., Serenelli A. M., Southworth J., 2014, A&A, submitted
- McQuillan A., Mazeh T., Aigrain S., 2013, ApJ, 775, L11
- Nordström B. et al., 2004, A&A, 418, 989
- Pollacco D. L. et al., 2006, PASP, 118, 1407
- Popper D. M., 1997, AJ, 114, 1195
- Queloz D. et al., 2000, A&A, 354, 99
- Santos N. C., Israelian G., Mayor M., 2004, A&A, 415, 1153
- Serenelli A. M., Bergemann M., Ruchti G., Casagrande L., 2013, MNRAS, 429, 3645
- Southworth J., 2011, MNRAS, 417, 2166
- Spada F., Demarque P., Kim Y.-C., Sills A., 2013, ApJ, 776, 87
- Tegmark M. et al., 2004, Phys. Rev. D, 69, 103501
- Teitler S., Königl A., 2014, ApJ, 786, 139
- Triaud A. H. M. J. et al., 2010, A&A, 524, A25+
- Weiss A., Schlattl H., 2008, Ap&SS, 316, 99
- Winn J. N., Fabrycky D., Albrecht S., Johnson J. A., 2010, ApJ, 718, L145
- Zhang M., Penev K., 2014, ApJ, 787, 131

Table 6. System parameters

Parameter (Unit)	WASP-87	WASP-108	WASP-109	WASP-110	WASP-111	WASP-112
Stellar parameters, including from the spectra:						
Constellation	Centaurus	Centaurus	Libra	Sagittarius	Capricornus	Piscis Austrinus
Right Ascension	12 ^h 21 ^m 17 ^s .92	13 ^h 03 ^m 18 ^s .73	15 ^h 28 ^m 13 ^s .23	20 ^h 23 ^m 29 ^s .55	21 ^h 55 ^m 04 ^s .23	22 ^h 37 ^m 57 ^s .43
Declination	-52°50′27″.0	-49°38′22″.8	-16°24′38″.8	-44°03′30″.3	-22°36′45″.2	-35°09′13″.9
V_{mag}	10.7	11.2	11.4	12.3	10.3	13.3
K_{mag}	9.6	9.8	10.2	10.7	9.0	11.9
Spectral type	F5	F9	F4	G9	F5	G6
T_{eff} (K)	6450 ± 120	6000 ± 140	6520 ± 140	5400 ± 140	6400 ± 150	5610 ± 130
log g_* (cgs)	4.32 ± 0.21	4.15 ± 0.20	4.3 ± 0.2	4.1 ± 0.2	4.0 ± 0.2	4.3 ± 0.2
ξ_t (km s ⁻¹)	1.34 ± 0.13	1.2 ± 0.1	1.6 ± 0.1	0.9 ± 0.1	1.5 ± 0.1	1.0 ± 0.1
v_{mac} (km s ⁻¹)	5.9 ± 0.6	4.4 ± 0.6	6.5 ± 0.6	3.3 ± 0.6	6.3 ± 0.6	3.2 ± 0.6
$v \sin i_*$ (km s ⁻¹)	9.6 ± 0.7	4.7 ± 0.8	15.4 ± 1.0	0.2 ± 0.6	11.2 ± 0.8	2.0 ± 1.4
[Fe/H]	-0.41 ± 0.10	+0.05 ± 0.11	-0.22 ± 0.08	-0.06 ± 0.10	+0.08 ± 0.08	-0.64 ± 0.15
log A(Li)	2.17 ± 0.08	2.70 ± 0.12	< 1.1	< 0.6	2.27 ± 0.11	< 0.7
Age _{evol} (Gyr)	3.8 ± 0.8	4.6 ± 1.9	2.6 ± 0.9	8.6 ± 3.5	2.6 ± 0.6	10.6 ± 3.0
Distance (pc)	240 ± 20	220 ± 15	330 ± 30	320 ± 30	210 ± 20	450 ± 30
Parameters from the MCMC analyses:						
P (d)	1.6827950 ± 0.0000019	2.6755463 ± 0.0000021	3.3190233 ± 0.0000042	3.7783977 ± 0.0000031	2.3109650 ± 0.0000024	3.0353992 ± 0.0000038
T_c (HJD-2450000)	6361.84030 ± 0.00021	6413.79019 ± 0.00015	6361.19263 ± 0.00023	6502.72413 ± 0.00016	6275.75127 ± 0.00040	6505.48734 ± 0.00013
T_{14} (d)	0.12436 ± 0.00071	0.13216 ± 0.00052	0.11856 ± 0.00098	0.11658 ± 0.00084	0.1373 ± 0.0017	0.11987 ± 0.00060
$T_{12} = T_{34}$ (d)	0.01516 ± 0.00087	0.01337 ± 0.00054	0.0237 ± 0.00010	0.01685 ± 0.00095	0.0174 ± 0.0017	0.01642 ± 0.00069
a/R_*	3.894 ± 0.095	7.05 ± 0.13	7.40 ± 0.13	11.15 ± 0.27	4.57 ± 0.20	8.19 ± 0.15
R_p^2/R_*^2	0.00765 ± 0.00013	0.01181 ± 0.00015	0.01213 ± 0.00019	0.02085 ± 0.00031	0.00644 ± 0.00019	0.01493 ± 0.00017
b	0.604 ± 0.028	0.19 ± 0.10	0.737 ± 0.011	0.376 ± 0.059	0.665 ± 0.037	0.475 ± 0.031
i_p (°)	81.07 ± 0.63	88.49 ± 0.84	84.28 ± 0.19	88.06 ± 0.35	81.61 ± 0.82	86.68 ± 0.28
K_1 (m s ⁻¹)	325 ± 14	117.8 ± 3.5	109 ± 15	71.8 ± 8.2	212 ± 14	142 ± 17
γ (m s ⁻¹)	-14 184.5 ± 7.9	47 073.925 ± 2.5	-16 643 ± 11	-34 821.9 ± 6.9	-19 800 ± 11	-19 587 ± 11
e	0 (adopted; < 0.099 at 2 σ)	0 (adopted; < 0.075 at 2 σ)	0 (adopted; < 0.32 at 2 σ)	0 (adopted; < 0.61 at 2 σ)	0 (adopted; < 0.10 at 2 σ)	0 (adopted; < 0.24 at 2 σ)
$v \sin i_p$ (km s ⁻¹)	—	—	—	—	11.12 ± 0.77	—
λ (°)	—	—	—	—	-5 ± 16	—
M_* (M_\odot)	1.204 ± 0.093	1.167 ± 0.092	1.203 ± 0.090	0.892 ± 0.072	1.50 ± 0.11	0.807 ± 0.073
R_* (R_\odot)	1.627 ± 0.062	1.215 ± 0.040	1.346 ± 0.044	0.881 ± 0.035	1.85 ± 0.10	1.002 ± 0.037
log g_* (cgs)	4.096 ± 0.023	4.336 ± 0.018	4.260 ± 0.018	4.498 ± 0.022	4.081 ± 0.036	4.342 ± 0.018
ρ_* (ρ_\odot)	0.280 ± 0.021	0.655 ± 0.034	0.493 ± 0.027	1.301 ± 0.095	0.238 ± 0.031	0.801 ± 0.043
T_{eff} (K)	6480 ± 110	5960 ± 120	6520 ± 140	5360 ± 130	6470 ± 120	5650 ± 110
[Fe/H]	-0.41 ± 0.10	0.05 ± 0.11	-0.220 ± 0.080	-0.06 ± 0.10	0.081 ± 0.080	-0.64 ± 0.15
M_p (M_{Jup})	2.18 ± 0.15	0.892 ± 0.055	0.91 ± 0.13	0.510 ± 0.064	1.83 ± 0.15	0.88 ± 0.12
R_p (R_{Jup})	1.385 ± 0.060	1.284 ± 0.047	1.443 ± 0.053	1.238 ± 0.056	1.442 ± 0.094	1.191 ± 0.049
log g_p (cgs)	3.416 ± 0.032	3.093 ± 0.023	3.000 ± 0.063	2.881 ± 0.057	3.305 ± 0.054	3.153 ± 0.054
ρ_p (ρ_J)	0.823 ± 0.088	0.422 ± 0.033	0.303 ± 0.048	0.268 ± 0.042	0.61 ± 0.11	0.521 ± 0.073
a (AU)	0.02946 ± 0.00075	0.0397 ± 0.0010	0.0463 ± 0.0011	0.0457 ± 0.0012	0.03914 ± 0.00098	0.0382 ± 0.0011
T_p (K)	2322 ± 50	1590 ± 36	1695 ± 40	1134 ± 33	2140 ± 62	1395 ± 33

Iron abundances are relative to the solar values obtained by Asplund et al. (2009). v_{mac} values obtained using the calibration of Doyle et al. (2014). Spectral Type estimated from T_{eff} using the table in Gray (2008).